Available online at www.sciencedirect.com
SCIENCE DIRECT®
Journal of Sound and Vibration 278 (2004) 563–580
JOURNAL OF SOUND AND VIBRATION
www.elsevier.com/locate/jsvi

Real-time active suppression of scattered acoustic radiation

E. Friot*, C. Bordier

CNRS, Laboratoire de Mécanique et d'Acoustique, 31 Chemin Joseph Aiguier, 13402 Marseille, France

Received 30 September 2002; accepted 9 October 2003

Abstract

Active noise control usually aims at reducing the total acoustic pressure due to a noise source; it may also be used in principle to reduce the scattered acoustic radiation from a reflecting body in order to render it invisible to incident acoustic waves. In this paper, a real-time control strategy is introduced to achieve, with ordinary noise sources and sensors, the effective suppression of the noise scattered by a 3-D surface. Numerical simulations of 2-D and 3-D control are used to illustrate the potential of this control strategy. Preliminary experimental results are also given for the 1-D case of a rigid body inserted into a duct.

1. Introduction

Active noise control usually consists of driving secondary noise sources to reduce the *total* acoustic pressure coming from a primary noise source. In principle, it can also be used to reduce only the *scattered* radiation from a reflecting body impinged by an incident wave; this could render submarines or underwater mines invisible to detection sonar systems, which is of interest for military purposes. Active control of scattered noise may also help to build anechoic rooms with low cut-off frequencies; in this case, the secondary sources should cancel the noise reflections from the walls.

A proof of the feasibility of active suppression of scattered radiation can be found in Ref. [1]: an integral representation of the acoustic pressure shows that a continuous layer of monopole-and-dipole control sources can perfectly cancel the scattered noise; the source strengths can be computed if the pressure due to the incident wave is known. A practical application of this basic principle comes up against two difficulties: first of all effective control requires finite sets of sensors and actuators instead of continuous layers. Ref. [1] provides a list of works addressing the

*Corresponding author. Tel.: +33-4-91-164084; fax: +33-4-91-164080.
E-mail address: friot@lma.cnrs-mrs.fr (E. Friot).

0022-460X/$ - see front matter
doi:10.1016/j.jsv.2003.10.064

discretization of the integral formulation; a significant reduction of the scattered noise appears to be achievable if the finite number of sensors and actuators used for control is large enough. Secondly, in practice only the *total* acoustic pressure can be directly measured whereas computing the control sources strengths requires the knowledge of the scattered pressure. Therefore driving a finite set of real actuators for reduction of the scattered pressure is not straightforward; only partial experimental results are available. For example in Refs. [2,3], arrangements of three loudspeakers and three microphones were used to cancel noise at some minimization microphones without radiating noise back in the direction of an incoming sound wave. In this way, the reflections from any body downstream from the microphones are theoretically cancelled in the direction of the incident wave. Unfortunately, the noise scattered in other directions is not necessarily reduced and the control devices called *auto-directive control sources* can only deal with one incident wave in free-field.

Controlling the surface vibration of a scattering body with mechanical actuators has been more widely investigated: if the body surface velocity matches the normal acoustic velocity of an incoming wave, no reflection occurs. For example in Ref. [4], the use of piezo-composite coating is investigated to monitor the vibration of a submarine hull. In Ref. [5], local monitoring of the reflected noise was achieved by using a loudspeaker to drive a rigid surface impinged by an incident wave. Until now however, the local "impedance matching methods" have only allowed the attenuation of the specular reflection at a body surface and not the global control of the scattered field. In Refs. [6,7], a strategy for dispatching and driving many actuators at the surface of a submarine is introduced but practical problems such as the real-time identification of the incident noise with one or several primary sources remain. Again in these cases it is not easy in practice to identify the incident pressure around a 3-D body; driving the whole surface vibration with mechanical actuators is also problematic for large bodies.

In this context, the control strategy introduced here aims at reducing the noise scattered from any 3-D body in an arbitrary finite or infinite propagation medium; this strategy leads to a real-time control algorithm which can be used for control with conventional actuators and sensors such as, in air, ordinary microphones and loudspeakers. This strategy also allows the reduction of the scattered radiation when the incident sound comes from multiple sources.

In Section 2 of this paper, the theoretical basis of the proposed algorithm is introduced. The scattered pressure from a reflecting body is first expressed in terms of an integral of the total pressure at a surface enclosing the body. Discretization of this integral allows the estimation of the *scattered* radiation by the linear filtering of the *total* acoustic pressure and pressure gradient at some points of this surface, whatever the noise sources and the propagation medium are. From a theoretical point of view, the corresponding linear filters can be numerically computed if the propagation medium is perfectly known. However for real-time control, it is much more efficient and reliable to *identify* these filters from in situ preliminary measurements; an effective identification procedure is proposed in Section 2. Once the scattered radiation has been predicted from measurements of the total acoustic pressure around the body, a modified version of the Filtered-X Least Mean Squares control algorithm can be used to reduce the scattered radiation with conventional auxiliary noise sources. Eventually it is shown that one inner ring of sensors, one ring of actuators and one outer ring of sensors allow a real-time implementation of the control strategy; this arrangement of sensors and actuators can also reduce the noise radiated from a body vibrating because of internal sources.

In Section 3, numerical simulations of the proposed control strategy are performed. Control of the radiation scattered by an infinite rigid cylinder and a parallelepiped are considered successively. One point of concern for practical applications is the number of actuators and sensors which are effectively required for control; simulations show that about three sensors per wavelength are needed around the reflecting body. About the same number of actuators and of outer sensors are required for an efficient control of the scattered radiation.

In Section 4, experimental results of scattered radiation reduction are given for a rigid body inserted into a duct. The real-time control algorithm was implemented on COMPARS, the LMA hardware system for control. A 15 dB reduction of the scattered noise was achieved in the 80–800 Hz frequency range. A parallel version of the real-time algorithm is currently being implemented for full 3-D control. In the conclusion of the paper, the applicability of real-time reduction of the scattered radiation to industrial problems is discussed.

2. Theory of the control algorithm

Active noise control can be efficiently implemented when a reference signal (correlated with the noise source to fight against) and error signals (e.g. acoustic pressure measurements at minimization locations) are available. In this case, a feedforward adaptive real-time algorithm such as the Filtered-X Least Mean Squares algorithm can be used to monitor the secondary sources (cf. Ref. [1]). Unfortunately, no error signal can be directly measured to account for the scattered acoustic radiation. The scattered noise is the difference between the acoustic pressure with the scattering body and the pressure without the body; it cannot be measured if the incident acoustic wave is unknown as in the case of a concealed submarine. Since the incoming detection noise may also come from multiple and unknown sources, no obvious reference signal is available either.

In this section, it is shown how proper error and reference signals can nevertheless be computed from acoustic pressure measurements around a scattering body; with an adequate arrangement of actuators and sensors, these signals can feed an adaptive control algorithm to reduce the scattered acoustic radiation in all directions, whatever the incident noise is.

2.1. Computation of error signals

In the frequency domain, the scattered acoustic pressure radiation p_s can classically be defined as an integral on a surface S enclosing a scattering body [8]:

$$\begin{aligned} p(\mathbf{r},\omega) &= p_i(\mathbf{r},\omega) + p_s(\mathbf{r},\omega) \\ &= p_i(\mathbf{r},\omega) + \int_S [G(\mathbf{r},\mathbf{r}_0,\omega)\nabla p(\mathbf{r}_0,\omega)\cdot\mathbf{n} - p(\mathbf{r}_0,\omega)\nabla G(\mathbf{r},\mathbf{r}_0,\omega)\cdot\mathbf{n}]\,\mathrm{d}S_0, \end{aligned} \tag{1}$$

where p is the *total* pressure and p_i is the *incident* pressure (the total pressure which could be measured if the scattering body were not present). G denotes the Green function for the propagation medium *without* the scattering surface.

Eq. (1) shows that a linear operator maps the total acoustic pressure around the scattering surface to the scattered pressure at any place outside the surface. This operator does not depend

on the incident field nor the acoustic field inside surface S; this means that the scattered pressure can be computed from practical measurements (with ordinary sensors) of the total acoustic pressure around the scattering body, whatever the incident waves are. In practice discretization of the integral in Eq. (1) with a finite number of sensors provides an approximation of the scattered pressure:

$$p_s(\mathbf{r}) \approx \sum_{k=1}^{N} [g_k(\mathbf{r},\omega)p(\mathbf{r}_k) + h_k(\mathbf{r},\omega)\nabla p(\mathbf{r}_k)\cdot\mathbf{n}_k]. \tag{2}$$

In the case of rigid scattering bodies, the normal acoustic velocity gradient vanishes at the body surface; if the k points of pressure measurements are close enough to the body surface, Eq. (2) therefore reduces to

$$p_s(\mathbf{r},\omega) \approx \sum_{k=1}^{N} g_k(\mathbf{r},\omega)p(\mathbf{r}_k,\omega). \tag{3}$$

In this case only pressure measurements are required to compute the scattered radiation. The paper will now consider only rigid scattering bodies in order to alleviate the derivation of the control algorithm; the strategy presented here also applies to non-rigid bodies but sensors for the normal pressure gradient would also have to be considered for the general case.

Let p_1 denote the noise radiated from the primary source at an arbitrary point. p_1 is the sum of incident pressure p_{1i} and of scattered pressure p_{1s}, as shown in Fig. 1. When secondary sources are brought in for control, only the scattered radiation of primary noise p_{1s} must be cancelled by the total (i.e. incident plus scattered) radiation of the secondary sources p_2 therefore a natural error signal for control would be $e(\mathbf{r},\omega) = p_{1s} + p_2$, which cannot be directly measured in real-time.

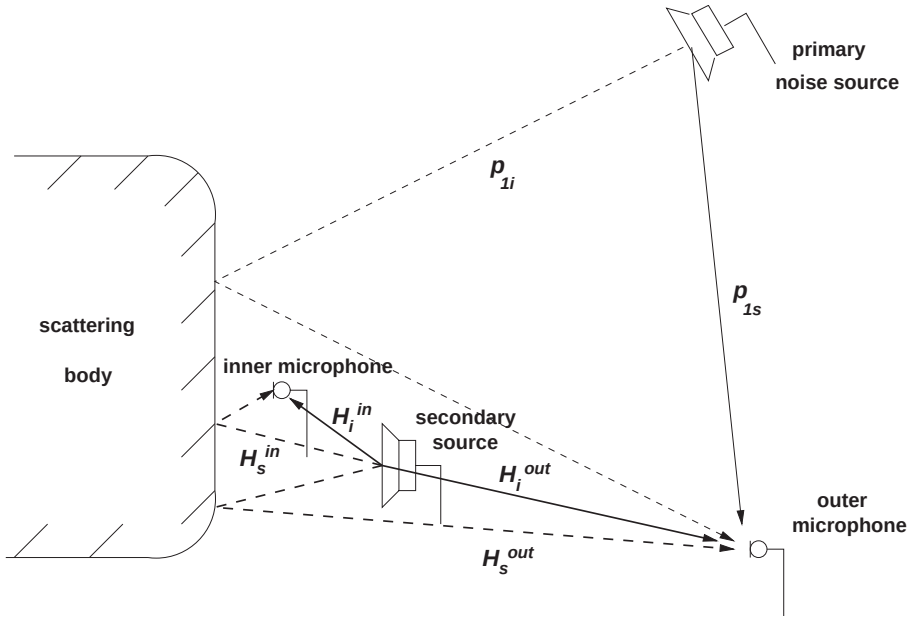

Fig. 1. Notations for the primary noise and the secondary paths.

Eq. (3) however allows e to be rewritten as

$$e(\mathbf{r},\omega) = p_2(\mathbf{r},\omega) + p_{1s}(\mathbf{r},\omega) \approx p_2(\mathbf{r},\omega) + \sum_{k=1}^{N} g_k(\mathbf{r},\omega) p_1(\mathbf{r}_k,\omega)$$

$$\approx p_2(\mathbf{r},\omega) + \sum_{k=1}^{N} g_k(\mathbf{r},\omega)[p(\mathbf{r}_k,\omega) - p_2(\mathbf{r}_k,\omega)]. \quad (4)$$

Alternatively, if the total secondary noise p_2 is also written as the sum of the incident pressure p_{2i} and of the scattered pressure p_{2s}, e can be rewritten as

$$e(\mathbf{r},\omega) = p_{2i}(\mathbf{r},\omega) + p_{2s}(\mathbf{r},\omega) + p_{1s}(\mathbf{r},\omega) = p_{2i}(\mathbf{r},\omega) + p_s(\mathbf{r},\omega)$$

$$\approx p_{2i}(\mathbf{r},\omega) + \sum_{k=1}^{N} g_k(\mathbf{r},\omega) p(\mathbf{r}_k,\omega). \quad (5)$$

In these equations, the acoustic pressures due to the secondary sources $p_2(\mathbf{r},\omega)$, $p_2(\mathbf{r}_k,\omega)$ and $p_{2i}(\mathbf{r},\omega)$ can be computed in real-time from the knowledge of the frequency response functions between secondary sources and sensors. Therefore, provided coefficients g_k are known, Eqs. (4) and (5) are two methods for computing in real-time error signals accounting for the scattered acoustic radiation.

2.2. Identification of the scattering filters

The linear filters g_k in Eqs. (4) and (5) can be computed by discretization of Eq. (1) from the propagation medium Green function, which may be difficult to obtain. However, for real-time control, it is easier and more accurate to identify these filters from measurements before control. An arbitrary set of incident waves can be generated before control with or without the scattering body, enabling the measurement of the scattered acoustic pressure by difference. In particular, it is convenient in practice to generate noise before control with each of the secondary sources and to measure the acoustic pressure at the minimization points in order to estimate the filters g_k from these measurements. As shown in Fig. 1 this can be done by surrounding the scattering body with two sets of sensors, one at the scattering body surface and one outside the set of actuators. Let $\mathbf{H}^{out}$ denote the matrix of frequency response functions between the actuators and sensors located at minimization points. Let also $\mathbf{H}_i^{out}$ denote the same FRF without the scattering body and $\mathbf{H}^{in} = \mathbf{H}_i^{in} + \mathbf{H}_s^{in}$ the FRF from the actuators to the inner sensors at the scattering body surface. The transfer matrix $\mathbf{G}$ between the total noise at the body surface and the scattered noise at the error sensors can be identified by minimizing the error index

$$J_G = \|\mathbf{H}_s^{out} - \mathbf{G}\mathbf{H}^{in}\|^2 = \|\mathbf{H}^{out} - \mathbf{H}_i^{out} - \mathbf{G}\mathbf{H}^{in}\|^2. \quad (6)$$

Matrix $\mathbf{G}$ is uniquely defined as soon as there are more actuators for identification than sensors at the body surface.

This identification of the scattering filters requires a set of sensors at the places where minimization of the scattered radiation is intended. It also requires FRF $\mathbf{H}_i^{out}$, which involves measurements of noise without the scattering body. This may not be feasible for some applications; in this case a computed version of $\mathbf{H}_i^{out}$ could be used in Eq. (6) to identify $\mathbf{G}$. By

contrast, $\mathbf{H}^{out}$ and $\mathbf{H}^{in}$, which may be difficult to compute for complex scattering bodies, can be easily measured.

2.3. Computation of a reference signal

The reference signal required for feedforward control must be linearly correlated with the error signals; it must detect the primary noise before it reaches the error signals and, to ensure stability, it must not be altered too much by control. When noise comes from several uncorrelated sources, several reference signals are usually required.

In the case of underwater applications, the source of the incident wave is a priori unknown. A reference signal must therefore account for waves coming from all directions. A simple way to compute a single reference signal is by summing the signals from all the sensors at the scattering body surface. In this way, the reference signal will detect the incoming wave as soon as it reaches the body, whenever this wave comes from.

With one primary source, the reference and the error signals will be fully correlated since scattering is a linear process. The reference signal will be altered by control with the secondary sources but this acoustic feedback can be of limited importance since the sensors at the body surface are not minimization sensors; the actuators and sensors can be arranged so that acoustic feedback is not destabilizing.

In the case of multiple sources, each of the incident waves will be detected at the body surface but some coherence between the reference and the error signals may be lost if the phase shifts between reference and minimization sensors are not the same for all the primary sources. However at low frequency and for distant primary sources, this loss of coherence can be small enough so as not to prevent control from working properly [9].

2.4. Practical arrangement of actuators and sensors

In practice the efficiency of an active noise control device depends largely on the selection of suitable *finite* sets of actuators and sensors.

Firstly, in the case of scattered radiation, minimization signals must be computed at places all around the scattering body in order to reduce the scattered radiation in all directions. Since the total acoustic pressure and the incident pressure satisfy Helmholtz's homogeneous equation, the scattered pressure due to the primary source p_{1s} also satisfies $\nabla p_{1s} + k^2 p_{1s} = 0$. The unique solution to Helmholtz's equation with uniform zero pressure at the boundary and no noise source in the domain is identically zero in the whole domain. Therefore, if p_{1s} is actively cancelled on a surface enclosing the scattering body and the secondary sources, the scattered radiation will automatically be cancelled outside this minimization surface. In practice, this means that a finite set of error signals (accounting for the scattered pressure at discrete locations on the surface) can be computed to reduce the scattered radiation in all directions around a scattering body. In Section 3 numerical simulations will show how many error signals are required in practice for an effective reduction of the scattered radiation.

Secondly, the secondary sources must also control the scattered radiation in all directions. Eq. (1) shows that the scattered noise can be seen as coming from sources located on any surface enclosing the scattering body. Secondary sources can therefore be laid at the body

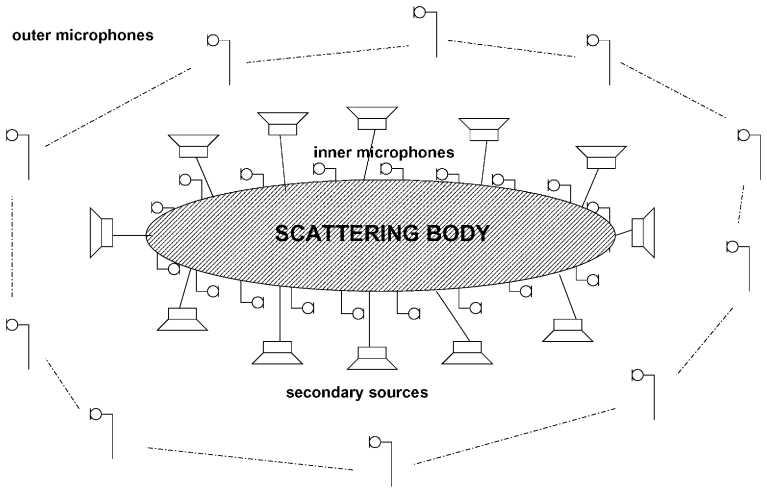

Fig. 2. Arrangement of actuators and sensors for real-time reduction of scattered radiation.

surface to counter the scattering sources. Alternatively, if the number of error signals is large enough to account for scattering in all directions, the same number of actuators may well reduce the scattered radiation wherever the actuators are. However for conditioning of the control problem [1] and causality, it is better to put the actuators all around the scattering body. Previous studies on global active noise control indicate that, in order to achieve a global reduction of the scattered noise outside the minimization ring, the secondary sources should be arranged so that the minimization sensors are in the far field of the sources (cf. Ref. [10]); in practice the corresponding minimum distance will depend on the size of the actual secondary sources.

Finally Fig. 2 displays a typical arrangement of actuators and sensors for real-time reduction of the scattered radiation. In air, microphones can act as sensors and loudspeakers as secondary sources. The inner sensors are used to compute an estimator of the scattered pressure according to Eqs. (4) or (5). By summation they also provide a single reference signal for real-time feedforward control. For control of random noise, the distance between the actuators and the inner sensors must be large enough so that the computation of the command signal takes less time than the noise propagation from the inner sensors to the actuators. The outer microphones are used before control to identify the scattering filters from Eq. (6); they can be removed for real-time control if the propagation medium is supposed to be stationary because in this case the scattering filters are invariant. If the scattering body were moving in an inhomogeneous medium, the outer microphones cannot be removed and on-line identification of the scattering filters would be necessary.

2.5. Real-time implementation of the control algorithm

Reference signal x and vector of error signals $\mathbf{e}$ can feed an adaptive real-time control algorithm. With a FXLMS algorithm, the command signal feeding the secondary source is $\mathbf{u} = \mathbf{W} * x$ where $*$ denotes the convolution product; the control finite impulse response filter $\mathbf{W}$ is

computed recursively as (cf. Ref. [11])

$$\mathbf{W}(n+1) = \mathbf{W}(n) - \alpha(\hat{\mathbf{H}}^{out} * x)\mathbf{e}(n), \tag{7}$$

where $\hat{\mathbf{H}}^{out}$ is a matrix of FIR filters approximating the FRF between the actuators and the error signals; α is a proper convergence coefficient.

Let $\hat{\mathbf{G}}$ denote a matrix of FIR filters accounting for the scattering filters identified as suggested in Section 2.2; with the error signal from Eq. (4), the updating formula for the filter controlling the scattered radiation is

$$\mathbf{W}(n+1) = \mathbf{W}(n) - \alpha(\hat{\mathbf{H}}^{out} * x)(\hat{\mathbf{G}} * [\mathbf{P}^{in} - \hat{\mathbf{H}}^{in} * \mathbf{u}] + \hat{\mathbf{H}}^{out} * \mathbf{u}), \tag{8}$$

where superscripts *in* and *out* distinguish the inner sensors from the outer ones in conformity with Figs. 1 and 2; $\hat{\mathbf{H}}$ denotes FIR approximation of the corresponding transfer matrix. Alternatively with the error signal from Eq. (5), the filter coefficients are updated according to

$$\mathbf{W}(n+1) = \mathbf{W}(n) - \alpha(\hat{\mathbf{H}}^{out} * x)(\hat{\mathbf{G}} * \mathbf{P}^{in} + \hat{\mathbf{H}}_i^{out} * \mathbf{u}). \tag{9}$$

Computation of the error signal from Eq. (4) requires one more convolution product than with Eq. (5); it was nevertheless used for the experiments of Section 4 because, in this case, the real-time algorithm is formally the same as the remote microphone technique (cf. Ref. [12]) previously implemented in the CNRS-LMA real-time control system.

Other adaptive algorithms may also be used for control of the scattered radiation. In particular, one convolution product can be saved if the Simplified RMT [13] or the filtered-error LMS algorithm [11] are used instead of the FXLMS. For example with the FELMS algorithm and Eq. (5), the filter coefficients can be updated according to

$$\mathbf{W}(n+1) = \mathbf{W}(n) - \alpha(\hat{\mathbf{H}}^{out\,\dagger} * \hat{\mathbf{G}} * \mathbf{P}_{\tau}^{in} + \hat{\mathbf{H}}^{out\,\dagger} * \hat{\mathbf{H}}_i^{out} * \mathbf{u}_{\tau})x(n), \tag{10}$$

where $\hat{\mathbf{H}}^{out\,\dagger}$ is the transposed matrix of FIR filters built by time-reversing the FIR filters in $\hat{\mathbf{H}}^{out}$; $\mathbf{P}_{\tau}^{in}$ and $\mathbf{u}_{\tau}$ are the signals $\mathbf{P}^{in}$ and $\mathbf{u}$ delayed by the time length of the filters in $\hat{\mathbf{H}}$. In this way, the convolution of invariant filters can be combined into single FIR filters and eventually only two convolution products are required to update the filter coefficients for control of the scattered radiation.

3. Numerical simulations of the control strategy

In this section, numerical simulations are presented to assess the efficiency of the control strategy introduced in Section 2 to cancel the scattered noise. In particular, the approximation of the scattered pressure by a linear combination of total pressure measurements and the identification of the combination coefficients from prior measurements have to be tested. Since these approximations stem from discretization of integrals, the real question is the number of sensors and actuators required for control.

Initially, the control of the noise scattered by an infinite rigid cylinder impinged by a plane wave in free field was simulated; this case was chosen because the scattered noise can be easily computed and because the span of the control is easy to assess in 2-D. According to the set-up introduced in Fig. 2, the cylinder with radius a was surrounded for control simulation by actuators consisting of infinite monopole lines parallel to the cylinder at a distance of $0.05a$ from the surface; outer

pressure measurements at a distance of $0.1a$ from the surface are taken as minimization signals. In the simulations that follow, the number of actuators and sensors as well as the frequency are varied. Secondly, the 3-D case of a rigid parallelepiped was tested in order to confirm the 2-D results and to prepare a full-scale real-time experiment in an anechoic theater.

3.1. Acoustic scattering by an infinite cylinder

When an acoustic plane wave interferes with a rigid cylinder parallel to the wave fronts, the scattered pressure p_s at a point with cylindrical coordinates (ρ, ϕ) is given at angular frequency ω by (cf. Ref. [9])

$$p_s(\rho,\phi) = -\mathrm{i}\omega\rho_v \sum_{n=0}^{\infty} \varepsilon_n(-\mathrm{i})^n \frac{\mathrm{J}_n'(ka)}{\mathrm{H}_n'^{(1)}(ka)} \mathrm{H}_n^{(1)}(k\rho)\cos(n\varphi), \tag{11}$$

where k is the wave number and ρ_v the fluid density; J_n denotes the Bessel function of first kind and order n, $\mathrm{H}_n^{(1)}$ the first Hankel function, $\varepsilon_{n=0} = 1$ and $\varepsilon_{n\neq 0} = 2$. When the incident pressure is produced by an infinite line of monopoles parallel to the cylinder at co-ordinates $(\rho_0, \varphi = 0)$, the scattered pressure is given by

$$p_s(\rho,\phi) = \mathrm{i}\omega\rho_i \sum_{n=0}^{\infty} \varepsilon_n \left[\mathrm{J}_n(k\rho_{inf}) - \frac{\mathrm{J}_n'(ka)}{\mathrm{H}_n^{(1)\prime}(ka)} \mathrm{H}_n^{(1)}(k\rho_{inf})\right] \mathrm{H}_n^{(1)}(k\rho_{sup})\cos(n\varphi), \tag{12}$$

where $\rho_{inf} = \inf(\rho, \rho_0)$ and $\rho_{sup} = \sup(\rho, \rho_0)$. In free field, Eqs. (11) and (12) are adequate for computing the scattered noise up to $ka = 100$. About ka terms are required for convergence of Eq. (11); it appears that about $10ka$ terms are required for convergence of Eq. (12).

Eq. (11) provides the primary noise to cancel with active control. When added to the direct noise produced by a monopole line in free-field, Eq. (12) provides the frequency response function from one actuator to one pressure measurement which gives the secondary noise when multiplied by the command signal.

3.2. Control with perfect knowledge of the scattered radiation

Even with perfect knowledge of the radiation scattered from the cylinder, exact cancellation of the scattered noise cannot be achieved with a finite set of minimization sensors and actuators. The purpose of this section is to show, before discussing any control strategy, what are the physical bounds to active control of the noise scattered by an infinite cylinder.

Firstly, 32 equally spaced measurements of the scattered pressure are taken around the cylinder as a minimization signal vector $\mathbf{P}_s$. Thirty-two monopole lines are also used for control; in order to avoid a loss of commandability due to symmetry, the first actuator and the first sensors are shifted by $2\pi/(3 \times 32)$ radian around the cylinder. By denoting $\mathbf{H}_{i+s}$ as the matrix of FRF from the actuators to the sensors, the command signal to exactly cancel the minimization signal vector $\mathbf{P}_s$ is $\mathbf{u} = -(\mathbf{H}_{i+s})^{-1}\mathbf{P}_s$. The scattered noise can be computed with or without this control by using Eqs. (11) and (12). Fig. 3 shows the directivity pattern of the scattered noise with or without control in the far-field, at a distance of $1000a$ from the cylinder, for $ka = 10$ and 15. The incident noise is a plane wave with amplitude 1 coming from the right at angle $\phi = 0$, as indicated by the arrow in the diagram. It can be seen that the scattered noise is largely reduced in all directions for

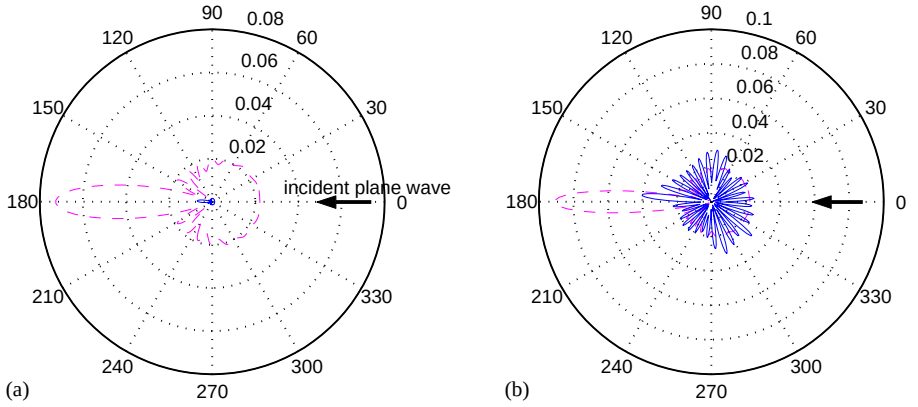

Fig. 3. Directivity pattern of the scattered noise with perfect knowledge control and 32 error signals, (a) $ka = 10$ and (b) $ka = 15$, — control on, - - control off.

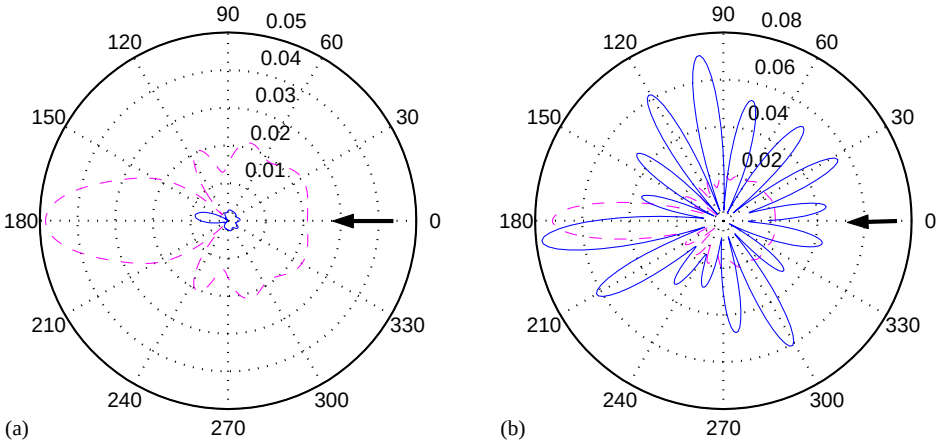

Fig. 4. Directivity pattern of the scattered noise with perfect knowledge control and 16 error signals, (a) $ka = 5$ and (b) $ka = 10$, — control on, - - control off.

$ka = 10$ whereas control increases noise in some directions for $ka = 15$; for $ka = 10$ the scattered noise is in fact reduced by a factor larger than 20 in all directions, which implies an attenuation superior to 25 dB.

Fig. 4 shows the scattered noise when the actuator and sensor number is reduced to 16. In this case, control still works for $ka = 5$ but spillover occurs for $ka = 10$. Fig. 5 shows the control results when the incident plane wave is coming from $\phi = 2\pi/(3 \times 32)$ and $\phi = (2 \times 2\pi)/(3 \times 32)$ with 32 minimization signal and for $ka = 10$; the control efficiency does not depend on the plane wave incidence angle.

In conclusion from the figures shown in this section, it appears that more than two minimization signals per wavelength are required around the cylinder for control of the noise scattered in all directions; three sensors per wavelength allow a noise reduction superior to 25 dB.

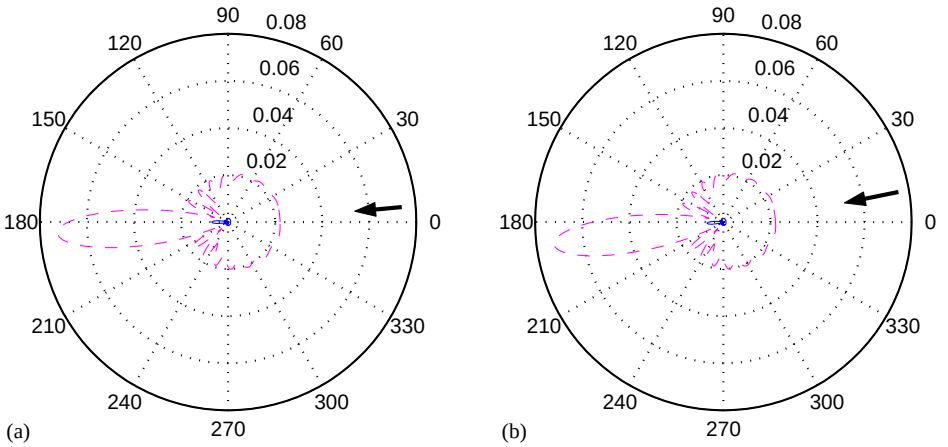

Fig. 5. Directivity pattern of the scattered noise with perfect knowledge control, 32 error signals and $ka = 10$, for two different incidence angles of the primary noise, (a) $\phi = \pi/48$ and (b) $\phi = \pi/24$.

3.3. Ideal estimation of the scattered radiation

For the simulations of this section, a set of inner pressure sensors is set up at $\rho = 1.01a$ around the cylinder, according to Fig. 2. As explained in Section 2.1, an estimate of the noise scattered by the cylinder can be computed from the signals provided by these sensors. The purpose of this section is to evaluate the number of sensors required for an accurate estimation of the scattered noise wherever the incident wave comes from.

For computer simulations, a large number of incident wave can be used to identify a matrix $\mathbf{G}$ which maps the pressure measurements around the cylinder to the scattered noise. If $\mathbf{P}_s^{out}$ denotes, for many incident waves, the matrix of the scattered noise at the outer sensors and $\mathbf{P}^{in}$ the total pressure at the inner sensors, matrix $\mathbf{G}$ can be identified by least square minimization of $||\mathbf{P}_s^{out} - \mathbf{G}\mathbf{P}^{in}||^2$.

Fig. 6 compares the exact scattered noise to the estimated one at 32 outer sensors when 32 inner sensors are used for estimation; for this simulation, 96 plane waves coming from all around the cylinder were used for identification of matrix $\mathbf{G}$. Because of the symmetry of the cylinder and of the identification of $\mathbf{G}$, the results in Fig. 6 do not depend on the incidence angle of the incoming plane wave. Fig. 7 shows the results obtained with 16 inner sensors and 16 outer sensors.

It can be seen from Figs. 6 and 7 that, with three sensors per wavelength at the cylinder surface, the scattered noise can be accurately estimated from total pressure measurement, wherever the incident wave comes from.

3.4. Control with estimation of the scattered radiation

In this section, active control is simulated to cancel the estimated scattered noise at the outer sensors; 32 outer sensors, 32 inner sensors and 32 actuators are used. Fig. 8 displays the directivity pattern in the far-field (in fact the pressure at a distance of $1000a$) of the scattered noise when control is used to cancel the estimation of this noise at the 32 outer signals. For the simulations

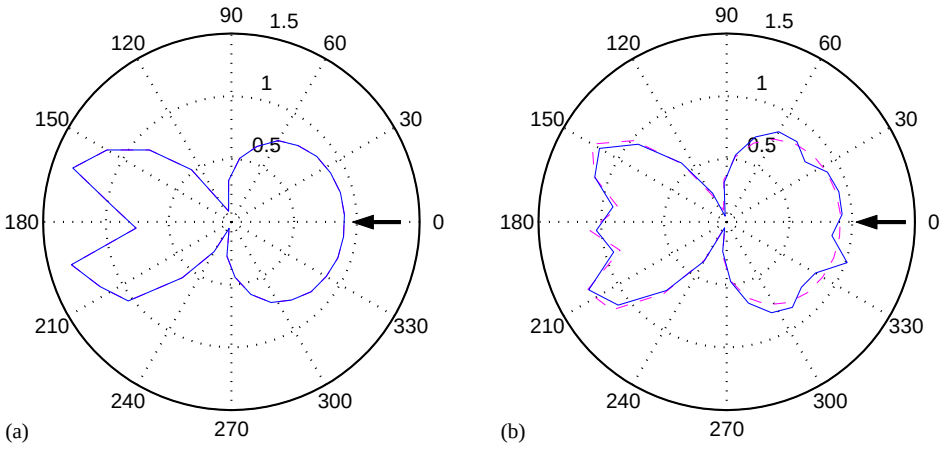

Fig. 6. Estimation with 32 inner sensors of the scattered noise at the minimization sensors, (a) $ka = 10$ and (b) $ka = 15$, — estimated, - - exact.

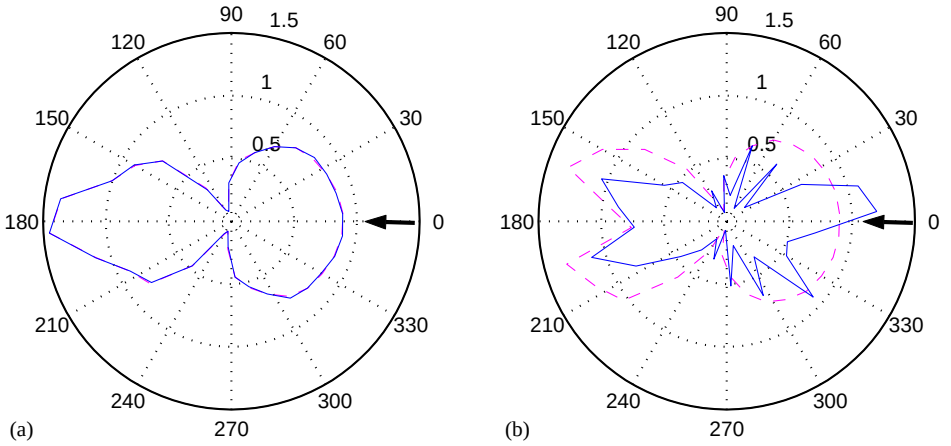

Fig. 7. Estimation with 16 inner sensors of the scattered noise at the minimization sensors, (a) $ka = 5$ and (b) $ka = 10$, — estimated, - - exact.

shown in Fig. 8, the matrix **G** mapping the total noise at the cylinder boundary to the scattered noise at the outer sensors was identified as in Section 3.3 from a large number of plane waves and a least-squares computation. It can be seen that control of the scattered noise is fully effective when three sensors per wavelength at the cylinder boundary are used.

In practice, as discussed in Section 2.2, the secondary sources can be used to generate noise for identification of the matrix **G** when the scattered noise cannot be computed a priori. Fig. 9 shows the control results when the error signals are computed with a matrix **G** in this way. In this case the control is slightly less effective, the estimation of the scattered noise is less accurate because matrix **G** was identified from cylindrical waves coming from the secondary sources and not from plane waves.

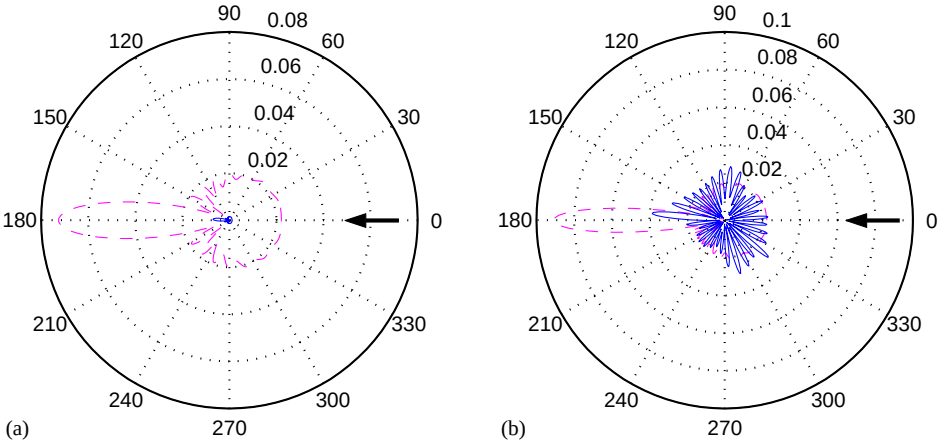

Fig. 8. Directivity pattern of the scattered noise with control of the ideally estimated scattered noise at 32 sensors, (a) $ka = 10$ and (b) $ka = 15$, — control on, - - control off.

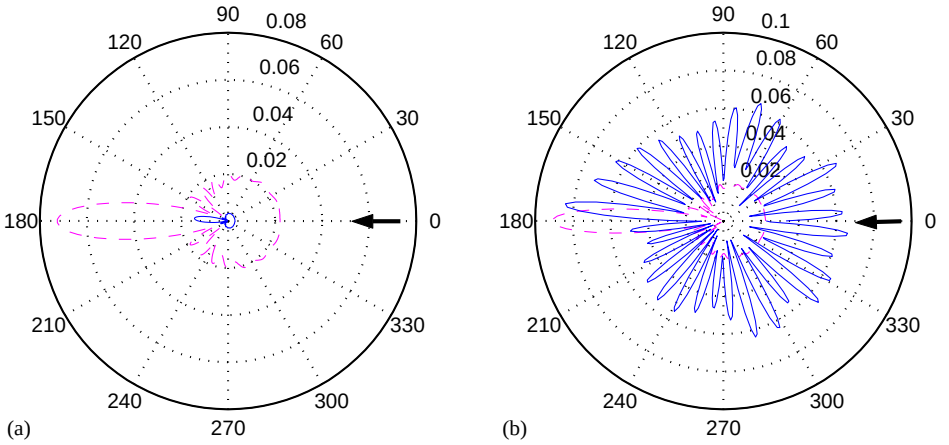

Fig. 9. Directivity pattern of the scattered noise with control of the practically estimated scattered noise at 32 sensors, (a) $ka = 10$ and (b) $ka = 15$, — control on, - - control off.

In conclusion, from the last three sections, it appears that the control strategy introduced in Section 2 is effective for control of the noise scattered by a rigid infinite cylinder provided that three sensors per wavelength at the cylinder boundary are used.

3.5. Simulation of 3-D control

The control strategy introduced for the scattered noise was also simulated in a 3-D case. The first objective of this simulation was to consider one particular case to determine whether the required number of sensors was also about three minimization sensors per wavelength in 3-D. The second objective of the 3-D simulation was to estimate the results which could be expected from a feasible 3-D practical laboratory experiment in an anechoic theater. The scattering body chosen

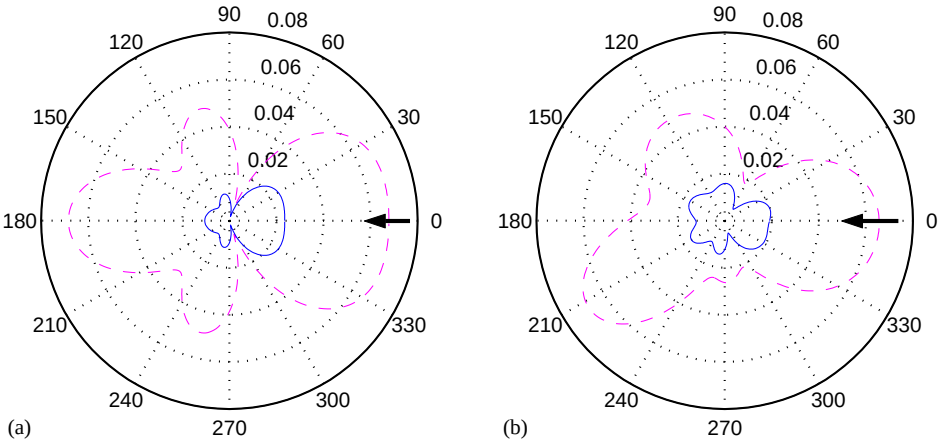

Fig. 10. Directivity pattern of the noise scattered by a parallelepiped impinged by a plane wave coming along a face (a) or an edge (b), — control on, - - control off.

for the simulation was a $1.6 \times 1 \times 1.2$ m rigid parallelepiped surrounded by 18 inner pressure sensors and 16 monopole sources, corresponding to the number of channels of the LMA real-time control system COMPARS. The minimization sensors were arranged in a single plane around the parallelepiped. An integral equation code was used to compute the noise around the parallelepiped and the control strategy introduced in Section 2 was numerically simulated. Fig. 10 shows the control results obtained in the minimization sensor plane for two incoming plane waves with a distinct incidence angle; the directivity patterns show the scattered acoustic pressure at 150 Hz at 10 m from the parallelepiped center. At this frequency there are about three minimization sensors per wavelength around the parallelepiped in the sensor plane. The control reduces the scattered noise in all directions but, because of the lack of actuators and sensors outside the plane of sensors, the reduction is not dramatic.

4. 1-D experimental results

The control strategy introduced in Section 2 was implemented for real-time control of the noise scattered by a tap at the end of a duct. Unlike previous experiments in ducts, active control was not invoked to cancel all the noise reflections at the tap; in this case, control was intended to *restore* in the duct the noise field that could be measured before inserting the tap, which did not correspond to an infinite duct because of the impedance break at the end of the duct. Fig. 11 roughly depicts the experimental set-up which is a 1-D reduction of the arrangement displayed in Fig. 2. The duct was a PVC cylinder with inner radius 7.5 cm. Control was intended in the 80–700 Hz range; below 80 Hz the loudspeakers used in the experiment were inefficient whereas 700 Hz was the highest frequency allowed by the real-time computations. During the experiment the primary source was fed by a 0–800 Hz white noise. A RMT algorithm (cf. Ref. [12]) implemented on the LMA control system COMPARS was used for control; the reference signal was directly taken from microphone 2.

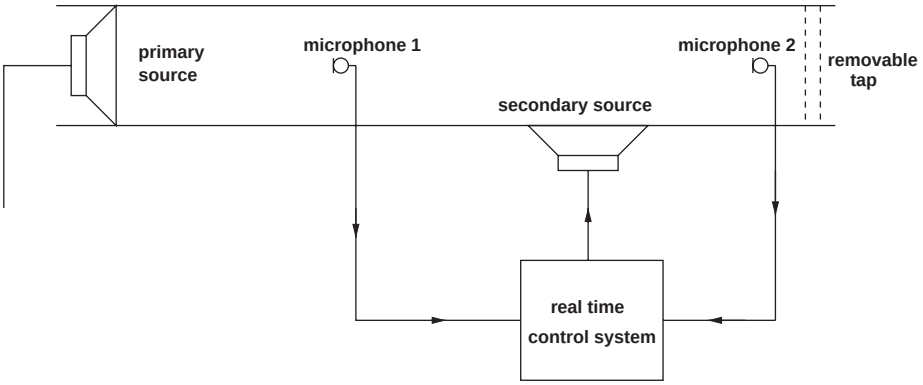

Fig. 11. Experimental set-up for real-time control of the scattered noise.

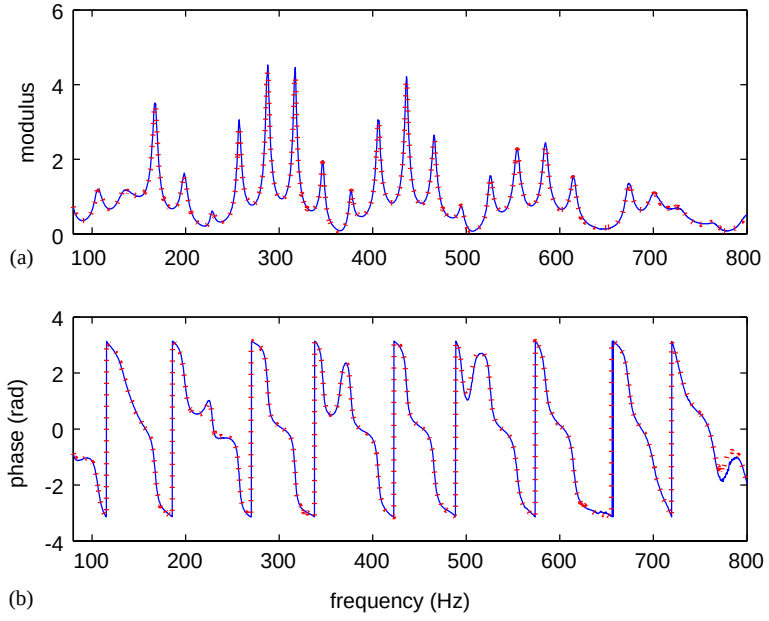

Fig. 12. The function **G** mapping the total noise at microphone 2 to the scattered noise at microphone 1, (a) modulus, (b) phase, — **G** identified with the primary source, - - **G** identified with the secondary source.

In this 1-D case, the matrix **G** mapping the total noise at microphone 2 to the scattered noise at microphone 1 is a single scalar function. **G** can be identified as indicated in Section 2.2 but, because the primary noise is perfectly known in this experiment, it can be computed in two ways depending on the noise source which is used for the identification process. Fig. 12 displays the function **G** which was identified with each of the noise sources. It can be seen that the two identified functions **G** overlap almost exactly, this suggests that the identification process is quite robust and that one can expect a good estimation of the scattered noise for control whatever the noise source is.

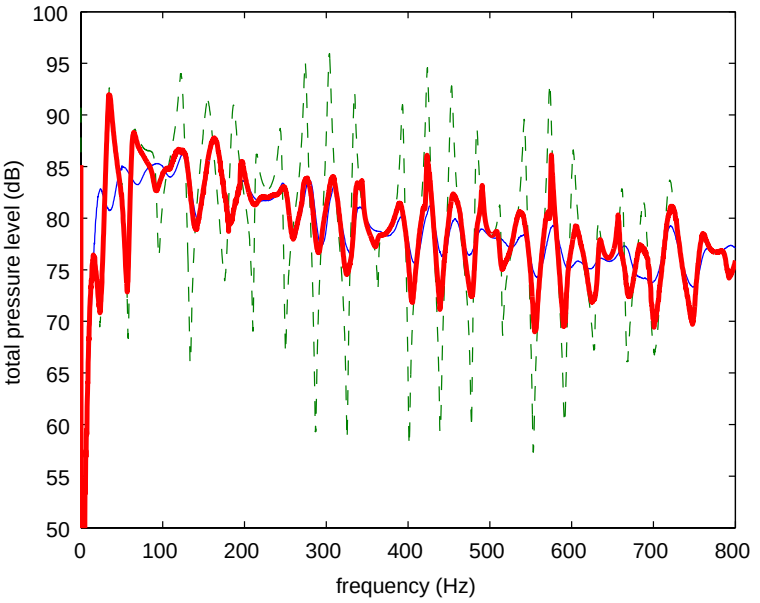

Fig. 13. Total noise at microphone 1, — without the tap, - - with the tap and control off, ▬ with the tap and control on.

Once matrix **G** has been identified, control of the scattered noise can be implemented. Fig. 13 displays the acoustic pressure level at microphone 1. Without the tap, weak resonances can be seen because of the partial reflections of the primary noise at the end of the duct. With the tap and without control strong resonances occur because the PVC tap is almost rigid. With the tap and with control, the noise at microphone 1 is close to the noise without the tap. Fig. 14 shows more precisely the scattered noise which is obtained by subtracting the noise without the tap to the noise with the tap. It can be seen that control reduced the scattered noise by 10–30 dB in the frequency range of interest.

5. Concluding remarks

In this paper, a control strategy has been introduced to achieve, with ordinary noise sources and sensors, real-time reduction of the acoustic radiation scattered by a reflecting body. Signals accounting for the scattered radiation can be computed from a set of total pressure measurements at the body boundary; a feedforward control relying on modified versions of the Filtered-X Least Mean Squares algorithm can then be used to reduce these error signals. Numerical simulations have shown that about three sensors per wavelength are required at the body boundary for an accurate estimation of the scattered noise in the case of a simple rigid body such as a cylinder. A 1-D real-time experiment have shown that, in the very simple case of a tap inserted into a duct, the control strategy is effective in practice.

The application of this control strategy to industrial cases is mainly restricted by the required number of sensors and actuators. For example, in the case of a submarine hiding from active

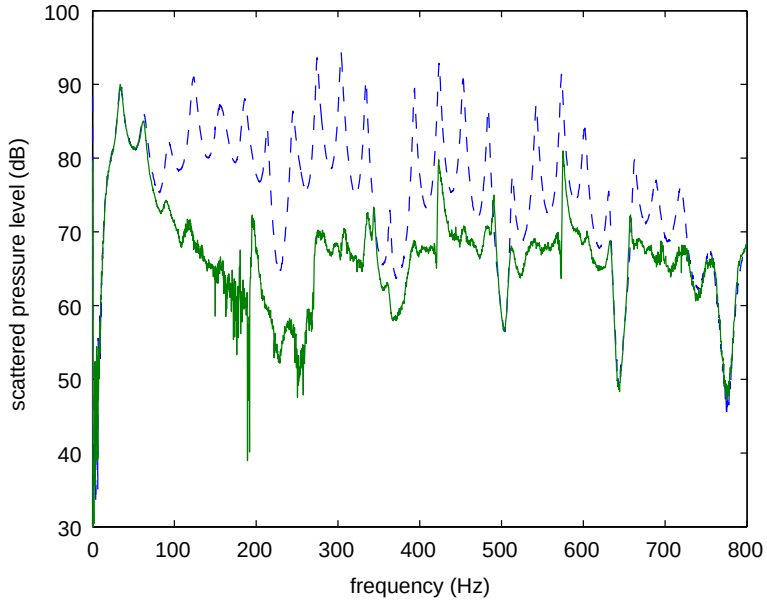

Fig. 14. Scattered noise at microphone 1, — control on, - - control off.

sonars, the distance between the sensors should be less than one meter; the resulting number of channels for a centralized control algorithm such as the one introduced here cannot be managed by today's standards. Three-dimensional simulations showed however that, with a reduced number of actuators and sensors, a reduction of the scattered noise might be observed on a small size experiment in an anechoic theater. Application to small objects such as underwater mines might then be considered, whereas for large reflecting bodies, application of scattered radiation control can be contemplated for low frequencies.

References

[1] P.A. Nelson, S.J. Elliott, *Active Control of Sound*, Academic Press, London, 1992, pp. 290–293.
[2] M. Hasebe, M. Kaida, Study on active noise attenuation in three-dimensional sound field, *Proceedings of Internoise 93*, Leuven, Belgium, 1993, pp. 773–775.
[3] G. Mangiante, A. Roure, Autodirective sources for 3D active noise control, *Proceedings of Internoise 94*, Yokohama, Japan, 1994, pp. 1293–1298.
[4] T. Howarth, V.K. Varadan, X. Bao, V.V. Aradan, Piezocomposite coating for active underwater sound reduction, *Journal of the Acoustical Society of America* 91 (2) (1992) 823–831.
[5] M. Furstoss, D. Thenail, M.A. Galland, Surface impedance control for sound absorption: direct and hybrid passive/active methods, *Journal of Sound and Vibration* 203 (1997) 219–236.
[6] B. Nayrolles, T. Nicolas, Conception of an active anechoic multicellular layer, *Proceedings of Active 97*, Budapest, Hungary, 1997, pp. 1179–1188.
[7] T. Nicolas, Conception d'une Couche Anéchoique Multicellulaire, Ph.D Thesis, Université de Rouen, 2000.
[8] J.J. Bowman, T.B.A. Senior, P.L.E. Uslenghi, *Electromagnetic and Acoustic Scattering by Simple Shapes*, Hemisphere, New York, 1987.

[9] E. Friot, C. Bordier, A free-field experiment of multichannel control for random noise coming from uncorrelated sources in an anechoic room, *Proceedings of Active 2002*, Southampton, UK, 2002, pp. 221–230.
[10] C. Bordier, Controle Actif Acoustique de Sources Inaccessibles, These de l'Universit de la Mediterrane, Paratre, 2003.
[11] S.J. Elliott, *Signal Processing for Active Control*, Academic Press, London, 2001.
[12] A. Roure, A. Albarrazin, The remote microphone technique for active noise control, *Proceedings of Active 99*, Fort Lauderdale, FL, 1999, pp. 1233–1244.
[13] E. Friot, A. Roure, M. Winninger, A simplified remote microphone technique for active noise control at virtual error sensors, *Proceedings of Internoise 2001*, Den Haag, Netherlands, 2001, pp. 681–684.